



Comparison studies of Zn-doped CuO thin films deposited by manual and automated nebulizer-spray pyrolysis systems and their application in heterojunction-diode fabrication

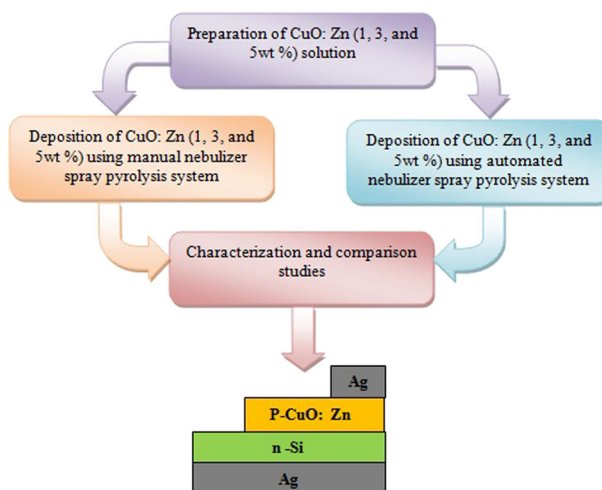
V. Jagadeesan¹ · Venkat Subramaniam¹

Received: 22 January 2021 / Accepted: 13 August 2021 / Published online: 1 September 2021
© The Author(s), under exclusive licence to Springer Science+Business Media, LLC, part of Springer Nature 2021

Abstract

This paper reports on the development of an automated nebulizer-spray pyrolysis (NSP) system and comparison studies of zinc-doped copper oxide with doping concentrations of 1%, 3%, and 5% deposited by manual and automated nebulizer-spray pyrolysis (NSP) systems for heterojunction-diode applications. The structural, optical, morphological, and electrical properties of the prepared manual and automated CuO:Zn thin films were compared. X-ray diffractometry (XRD) studies revealed that all the manual and automated CuO:Zn thin films have monoclinic structure. The crystallite size of the films has been calculated using Scherrer's formula. Field-emission scanning electron microscope (FESEM) images revealed spherical-shaped small grains in the automated CuO:Zn thin films, while agglomerated particles are observed in the manual CuO:Zn thin films. The highest optical absorbance and lowest optical band gap values were recorded using UV–Vis spectrophotometry. The optical band gap value increases when the doping with Zn increases beyond 3%. The maximum electrical conductivity of manual and automated CuO:Zn thin films was recorded using an electrometer. Based on the results obtained from these characterization studies, *p*-type (3% CuO:Zn thin film) and *n*-type (silicon wafer) samples prepared using the manual and automated NSP systems were used to fabricate Ag/*p*-CuO:Zn/*n*-Si heterojunction diodes, which were studied under dark and light conditions. The investigation results reveal that the heterojunction diode fabricated using the automated NSP system has a lower ideality factor and barrier height compared with the heterojunction diode prepared using the manual NSP system.

Graphical Abstract



✉ V. Jagadeesan
vjpsgcasl@gmail.com

¹ Department of Electronics, PSG College of Arts & Science, Coimbatore 14 Tamilnadu, India

Keywords Nebulizer-spray pyrolysis · Microcontroller · CuO:Zn thin film · Ag/p-CuO:Zn/n-Si heterojunction diode · Barrier height · Ideality factor

Highlights

- Manual and automated CuO:Zn (3%) thin films show good structural, optical, morphological, and electrical properties.
- Ag/p-CuO:Zn/n-Si heterojunction diode is fabricated using manual and automated nebulizer-spray pyrolysis (NSP) system.
- Automated Ag/p-CuO:Zn/n-Si heterojunction diode shows the lowest ideality factor (η) and barrier height (ϕ_b).
- The investigation results confirm that the automation process significantly modifies thin-film and diode properties.

1 Introduction

Thin films have been synthesized by a number of methods, such as successive ionic-layer adsorption and reaction (SILAR), chemical bath deposition, sol-gel, and spray-pyrolysis. Among these, the sol-gel method is a notable wet chemical way to synthesize oxide-based nanomaterials with high compositional homogeneity, which is considered an effective approach for modifying substrate surfaces [1]. Similarly, spray-pyrolysis techniques are also versatile chemical methods for synthesizing oxide-based nanomaterials [2]. In addition, obtaining a large surface area and a stable surface is a significant advantage of the sol-gel method. The spray-pyrolysis technique is also suitable for large surface area coating, and clean, adherent, pinhole-free, stable thin films can be obtained [3], with several reports of the formation of oxide-based nanomaterials by spray pyrolysis having appeared [4–7]. Spray pyrolysis is a cost-effective technique performed at low temperature to deposit thin films with uniform thickness on large surface areas. Thin-film deposition by spray pyrolysis has been applied in various devices such as sensors, solar cells, fuel cells, optoelectronic devices, and many others [8–12]. In spray pyrolysis, thin films are prepared by spraying a precursor solution onto a heated substrate, with the formation of uniform and fine droplets being crucial. Nozzle atomizers are used to achieve uniform and fine droplets in a controlled manner. However, some nozzle atomizers have limitations on the size and size distribution of the droplets obtained. In recent years, new or modified nozzle atomizers have been developed to overcome those limitations, such as air blast, electrostatic, ultrasonic nebulizer, and nebulizer-spray pyrolysis (NSP). Among the various nozzle atomizers, nebulizer-spray pyrolysis produces small droplets in the desired size range. Furthermore, this approach consumes less power than ultrasonic nebulizers. In the NSP technique, which is based on the Venturi principle, a precursor-solution is converted into an aerosol by the nebulizer. Various parameters affect the quality of the films, such as nozzle movement, the distance between nozzle and substrate, temperature, precursor

solution composition, etc. Among these, spray nozzle movement is an important parameter that affects the quality of the thin films. In the manual NSP system, variations in spray-nozzle movement lead to uneven spraying on the substrate. To overcome this problem, one possible improvement can be done by automating the spray-nozzle movement using a microcontroller. Recently, microcontroller-based automation in nebulizer spray pyrolysis has been developed to enhance the quality of the film, minimize human errors, and improve production efficiency [13–16].

Copper oxide (CuO) has generated significant interest as a promising semiconducting material due to its low band-gap, high abundance in nature, nontoxic nature, and monoclinic crystal structure [17, 18]. CuO is an excellent semiconducting material for the fabrication of p-type semiconductors. The deposition techniques and processing parameters used strongly influence the properties of CuO thin films. In addition, over the past few decades, there have been many reports of the impact of transition-metal (Zn, Ni, Co, and Mn) doping of CuO [19–22]. Among these dopants, the ionic radius of Zn^{2+} is close to that of Cu^{2+} (0.74 Å and 0.73 Å, respectively). Hence, the integration of Zn(II) into CuO will be favorable for optoelectronic applications [23, 24].

In the present work, the properties of zinc-doped copper oxide thin films with doping concentrations of 1, 3, and 5 % deposited using both a manual NSP system and an automated NSP system are compared and discussed. These materials are subsequently incorporated into Ag/p-CuO:Zn/n-Si heterojunction diodes and their properties are compared. Although some reports are available on the application of CuO for heterojunction diodes [25–27], there have been no prior studies comparing the properties of CuO:Zn thin films prepared by manual and automated NSP systems. In addition, to the best of our knowledge, no literature work has been reported on Ag/p-CuO:Zn/n-Si heterojunction-diode devices. This work will also provide researchers currently working in the thin-film and sol-gel field with a useful review of spray-pyrolysis deposition techniques.

Fig. 1 Schematic diagram of manual NSP systems

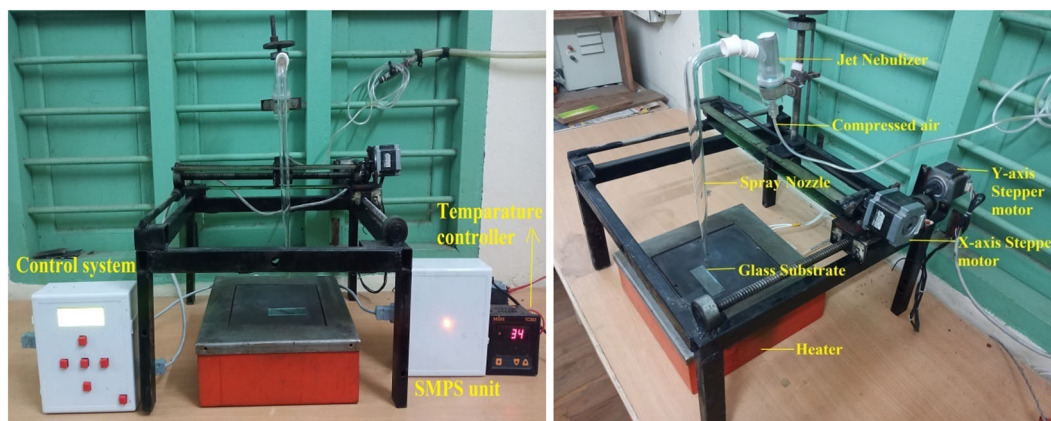
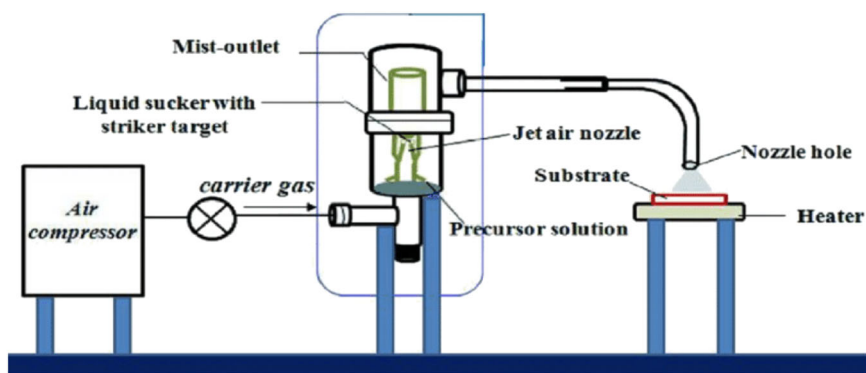


Fig. 2 Schematic diagram of automated NSP systems

2 Experimentation details

2.1 Deposition of Zn-doped CuO thin films by manual and automated NSP system

Precursor solutions were prepared by dissolving copper nitrate ($0.3 \text{ mole Cu(NO}_3)_2 \cdot 3\text{H}_2\text{O}$) and the required quantity of zinc nitrate ($\text{Zn(NO}_3)_2 \cdot 6\text{H}_2\text{O}$; 1, 3, or 5 wt% with respect to the quantity of $\text{Cu(NO}_3)_2 \cdot 3\text{H}_2\text{O}$) in 20 ml of double-distilled water and stirring continuously for 1 h using a magnetic stirrer. CuO:Zn thin films were produced using either a manual or automated NSP system, as described below. The former suite of sample is subsequently referred to as M1, M2, or M3 (where 1, 2, and 3, respectively, refer to the wt% of $\text{Zn(NO}_3)_2 \cdot 6\text{H}_2\text{O}$ in each solution), while the corresponding suite of samples prepared using the automated NSP system are identified as A1, A2, and A3.

In the manual NSP system (Fig. 1), a custom-designed glass tube with a 25 cm horizontal length and 10 cm vertical length was used as a solution-flow tube. The bottom of the glass tube is carefully designed as a spray nozzle with a 0.1 mm diameter attached to the nebulizer. The temperature of the substrate heater was initially set to 450°C and maintained using the temperature controller. The distance between

the nozzle and the glass substrate was fixed at 5 cm. Finally, 5 ml of the prepared solution was sprayed manually on the pre-cleaned glass substrate that was kept on the hot plate of the substrate heater.

In the automated NSP systems (Fig. 2), a custom-designed glass spray-nozzle, that is attached to the nebulizer, is used for the automatic deposition process. The nebulizer was fixed at the top of the x-axis carriage and the nebulizer was filled with 5 ml of the precursor solution. The distance between the nozzle and substrate was fixed at 5 cm. The spray nozzle was correctly positioned at the top of the glass substrate using dedicated keys in the control unit. An air compressor was used to generate a stream of air at a pressure of 2.1 kg/cm^2 , which impinges the solution situated inside the spray nozzle, thus atomizing the solution and directing the resulting liquid droplets onto the glass substrate. During deposition, the position of the spray nozzle is translated in the x- and y-axis directions via the microcontroller.

2.2 Fabrication of Ag/p-CuO:Zn/n-Si heterojunction diode

Fig. 3 shows the structure of the Ag/p-CuO:Zn/n-Si heterojunction diode fabricated in this work. A p-type CuO:Zn

thin film was deposited on a *n*-type silicon wafer using the manual and automated NSP system to form the p-CuO:Zn/*n*-Si device with front and back silver contacts.

Careful cleaning procedures were adopted to clean the silicon substrate, as per previous literature work [28]. Based on the optimized results (see below), a suitable p-CuO:Zn precursor composition was chosen and deposited on the polished side of the *n*-Si substrate using both manual and automated NSP systems. Ohmic contacts (Ag) were then deposited by a thermal evaporation technique on both the CuO:Zn and the rough side of the *n*-Si substrate.

2.3 Characterization techniques

The structural properties of the CuO:Zn thin films were studied and compared using X-ray diffraction (XRD) (Shimadzu XRD-6000, Japan) with Cu- $k\alpha_1$ radiation source of wavelength 1.5418 Å and grazing incident angle (GIXD) is fixed at $<5^\circ$ to focus on only the topmost surface of the film. Stylus profilometry (Mitutoyo SurfTest SJ-301) was used to measure the thickness of the films. The surface morphology and chemical composition of the films were observed and compared through high-resolution Schottky field-emission scanning electron-microscopy (FE-SEM) and energy-dispersive X-ray analysis (EDAX) (Tescan MIRA XMU

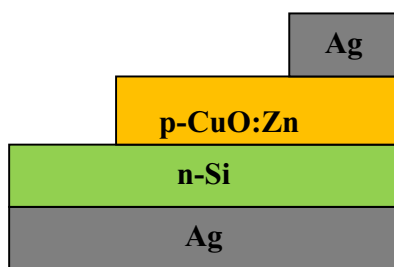


Fig. 3 Device structure of Ag/p-CuO:Zn/*n*-Si heterojunction diode

3.0). Optical properties such as absorbance, transmittance, and bandgap of the films were studied using UV–visible spectrophotometry (JASCO-570). The voltage–current (*V*–*I*) characteristics of the CuO:Zn thin films were measured using a Keithley electrometer (6517-B) in a two-probe setup over a voltage range of 1–10 V. The *V*–*I* characteristics of the Ag/p-CuO:Zn/*n*-Si heterojunction-diode were similarly studied under dark and light conditions (tungsten halogen and metal halide—100 mW/cm²) at room temperature.

3 Results and discussion

3.1 Structural studies

The X-ray diffraction patterns of the CuO:Zn thin films prepared using the manual and automated NSP systems are shown in Fig. 4. All observed diffraction peaks were assigned to the monoclinic crystal phase in accordance with standard JCPDS card No. 89-5899 [29]. Peaks were observed at 2θ angles of 32.6, 35.5, 38.7, and 52.7° corresponding to (110), (–111), (111), and (020) planes for both sample series, with samples M2 and A2 exhibiting the most well-defined patterns. No peaks corresponding to Zn-impurity phases are evident (Fig. 4), even at the highest dopant concentrations (M3 and A3). The results reveal that the zinc ions were successfully incorporated into the CuO structure [30]. The diffraction patterns obtained for the A-series samples are sharper and generally more intense than those observed for the M-series samples, consistent with the formation of more well-defined, crystalline films in the former case.

The various structural parameters of the CuO:Zn thin films are shown in Table 1. To obtain uniform thickness, the most important parameters that have been optimized in this study include substrate temperature, molarity of the

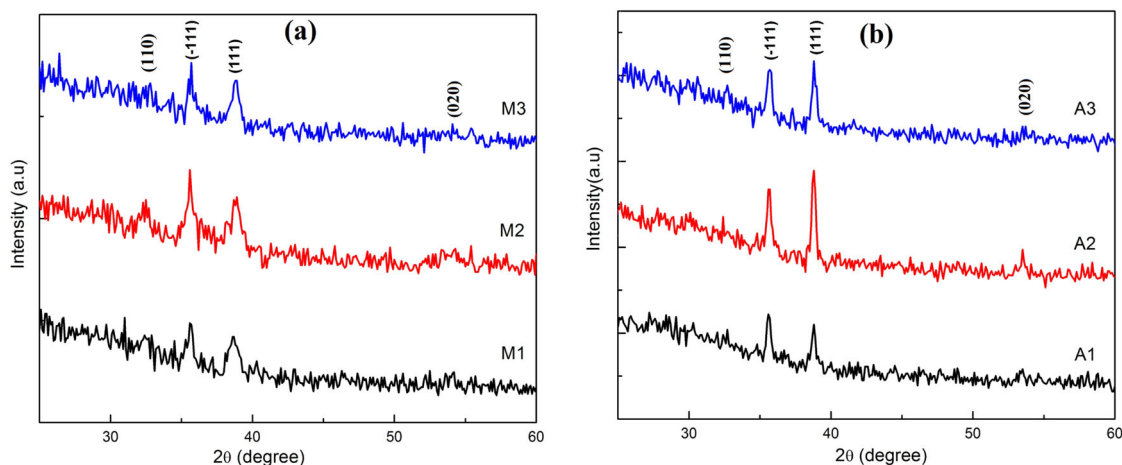
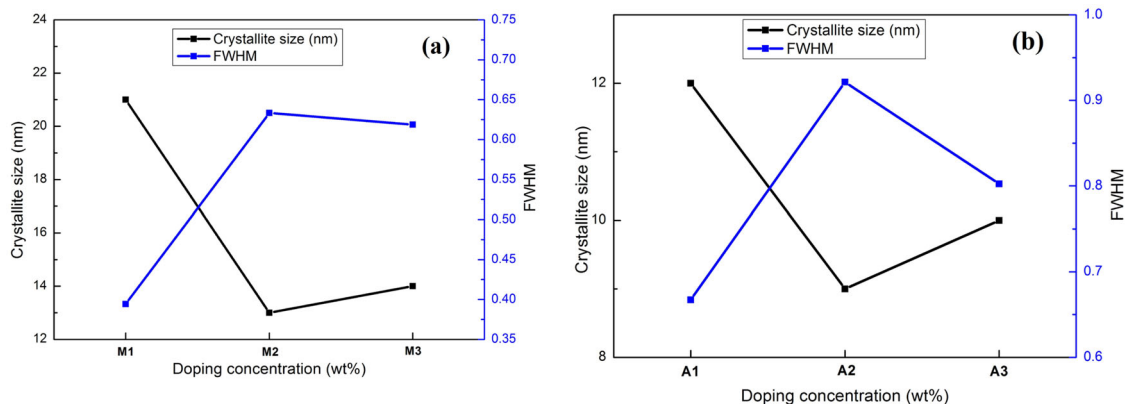


Fig. 4 XRD patterns of CuO:Zn thin films prepared using (a) manual and (b) automated NSP systems

Table 1 Various structural parameters of manual and automated CuO:Zn thin films

Samples	2θ (degree)	FWHM (degree)	Crystallite size (<i>D</i>) (nm)	Micro strain (ϵ)	Dislocation density (δ) ($\times 10^{15}$ lines m^{-2})	Average thickness (nm)
M1	38.7516	0.3942	21	0.0016	2.18919	112
M2	38.7583	0.6333	13	0.0026	5.64718	109
M3	38.8094	0.6188	14	0.0025	5.38985	105
A1	38.7764	0.6671	12	0.0027	6.2653	110
A2	38.7893	0.9214	9	0.0037	11.951	107
A3	38.6387	0.8025	10	0.0033	9.0744	104

**Fig. 5** Variation of crystallite size and FWHM as a function of doping concentration for CuO:Zn thin films prepared using (a) manual and (b) automated NSP systems

solution, nozzle-to-substrate distance, air pressure, spraying volume, and deposition time. The full width at half maximum (FWHM) is found to be the highest for samples M3 and A3. The crystallite size can be calculated using Scherrer's formula from the full width at half-maximum [31]. The crystallite size (*D*), microstrain (ϵ), and dislocation density (δ) was evaluated using the below formula:

$$D = \frac{0.9\lambda}{\beta\cos(\theta)} \quad (1)$$

$$\epsilon = \frac{\beta\cos\theta}{4} \quad (2)$$

$$\delta = \frac{1}{D^2} \quad (3)$$

where β , θ , λ , and *D* are full width at half-maximum, Bragg angle, X-ray wavelength, and evaluated crystallite size. Using the Scherrer formula, Fan et al. estimated the crystallite sizes of sol-gel-derived CuO produced in their work to be from 8 to 26 nm [32]. Rafea et al. also reported CuO crystallite sizes of 14–21 nm which is in good agreement with these results [33]. The crystallite size decreased for samples M2 and A2 because of the crystallinity improvement of CuO and ionic radius difference

between Cu^{2+} and Zn^{2+} [34]. The crystallite size is increased by increasing Zn doping concentration. Increasing crystallite size is accompanied by a decrease in dislocation density and microstrain. The lowest crystallite size is found to be 9 nm for sample A2 and similarly, the lowest crystallite size is 13 nm for sample M2, and also the highest value of microstrain and dislocation density has been calculated for M2 and A2.

The variations in crystallite size and FWHM for the CuO:Zn films with doping are illustrated in Fig. 5, while the corresponding microstrain data are shown in Fig. 6. It is evident that the minimum crystallite size is obtained for the M2 and A2 samples in each series. However, significantly smaller crystallites are obtained in the case of sample A2 (9 nm, compared with 13 nm for M2), reflecting the advantages of the automated approach in obtaining small crystallites.

3.2 Surface morphology and elemental composition

The FESEM images of CuO:Zn thin films produced using the manual NSP system (samples M1, M2, and M3) are shown in Fig. 7. The homogeneity and morphology of the films are similar to that reported by Meherun Nesa et al., with crack-free coatings composed of nonuniform

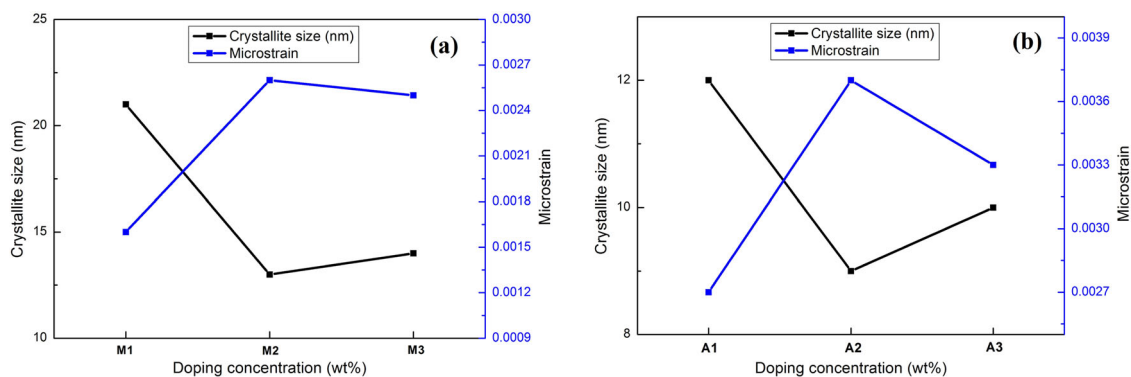


Fig. 6 Variation of crystallite size and microstrain as a function of doping concentration for CuO:Zn thin films prepared using (a) manual and (b) automated NSP systems

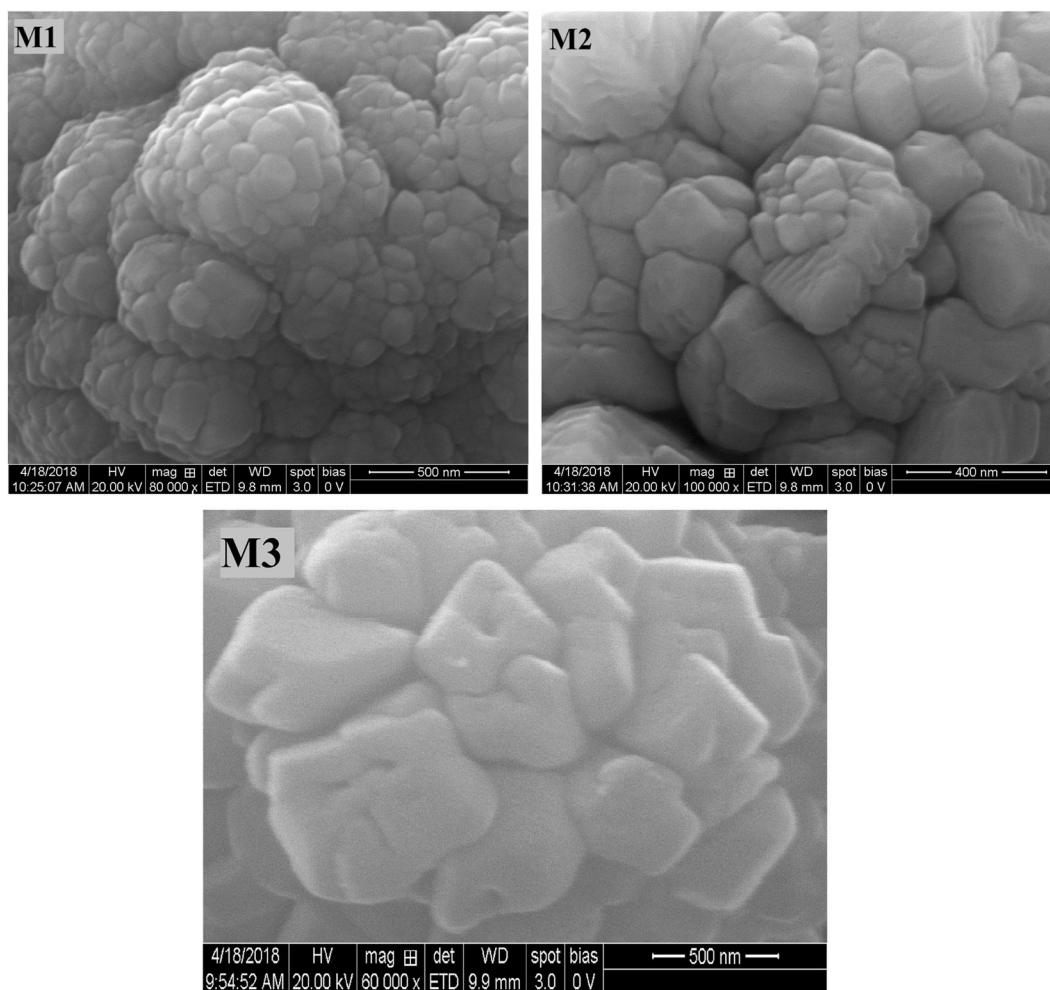


Fig. 7 FESEM images of CuO:Zn thin films produced using the manual NSP systems

nanosized particle agglomerates being evident [35]. A similar agglomerated morphology for such CuO:Zn coatings was also reported by Rejith et al. [36]. Overall, the distribution and formation of particles on the substrate is irregular, with different shapes being observed for all CuO:

Zn films produced using the manual NSP system, [37], indicating that the particles were not deposited uniformly.

The FESEM images of the CuO:Zn thin films produced using the automated NSP system are shown in Fig. 8. Generally, doping of CuO with Zn(II) does not have much

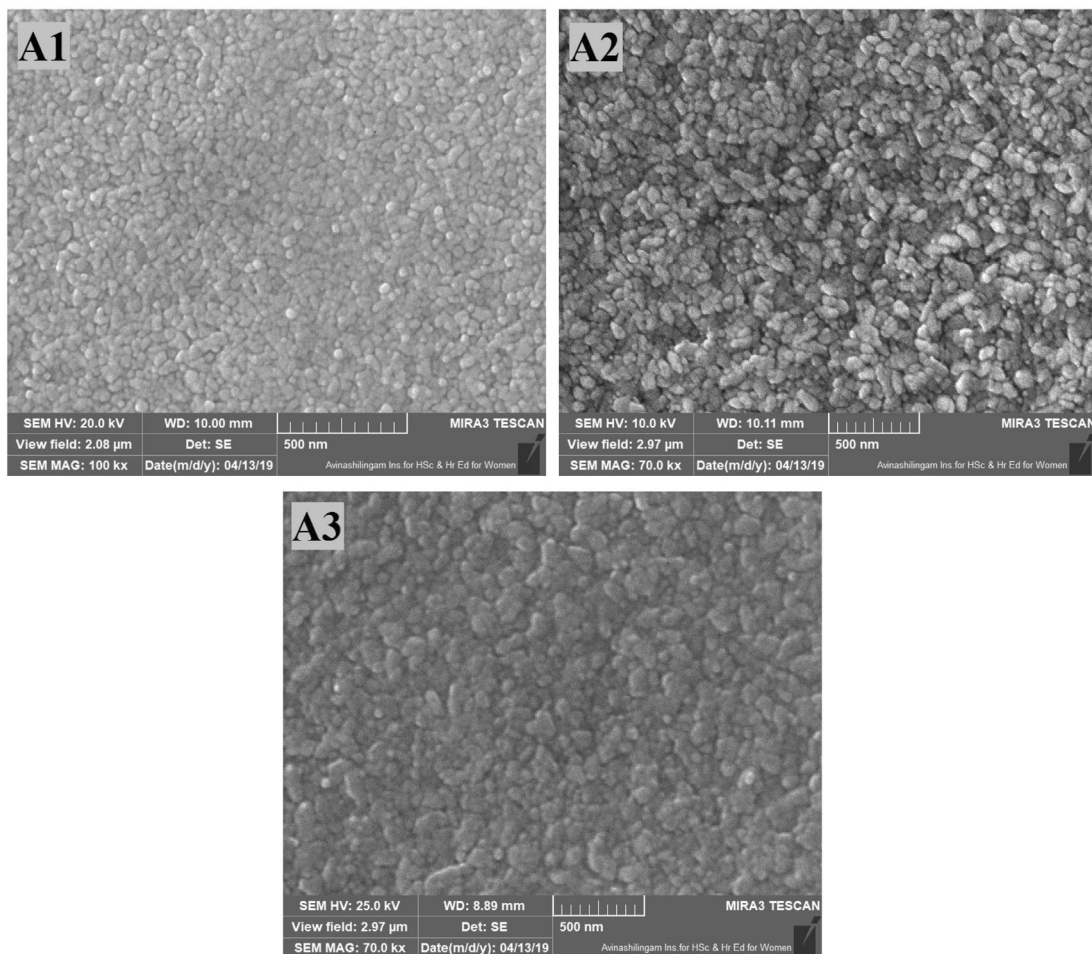


Fig. 8 FESEM images of CuO:Zn thin films produced using the automated NSP systems

impact on the morphology of CuO [38]. However, in the present work, samples A1, A2, and A3 exhibit small, uniform spherical particles. The particles are closely packed, with uniform, crack-free coatings being evident in all samples. In both the M- and A-series coatings, the particle size decreases as the dopant concentration is increased from 1 to 2%, and then increases with increasing dopant concentration. Variations of particle size seen in FESEM images are well correlated with the variations of crystallite size calculated from XRD studies [39].

In summary, the FESEM studies indicate that deposition employing the automated NSP system provides nanosized particles with uniform distribution at all dopant concentrations explored. In contrast, large, non-uniform and agglomerated particles were observed in the corresponding films produced using the manual NSP system.

Energy-dispersive X-ray spectra (EDS) of the samples were obtained to examine the purity and chemical composition of the materials, with the spectra obtained for films deposited using the manual and automated systems shown

in Figs. 9 and 10, respectively. As expected, the EDS data reveal the presence of Cu, O, and Zn atoms, with no other impurities being evident above the detection limits. As indicated in the tabulated data included in Figs. 9 and 10, samples M3 and A3 exhibit Zn concentrations of 0.69 and 0.92 at%, respectively.

3.3 Optical studies

The optical absorbance of the CuO:Zn thin films was analyzed in the wavelength range of 300–1200 nm, as shown in Fig. 11. These data indicate that sample A2 has the highest absorbance from 400 to 800 nm, with comparable absorbances being observed for all samples below 400 nm and above 900 nm. The absorbance of samples M1 and M2 is comparable within the spectral range explored. In both the M- and A series, the samples with the highest dopant concentrations exhibit the lowest absorbance from 400 to 800 nm.

The optical bandgap energy of the films was derived from the optical absorbance spectra via Tauc plots, as

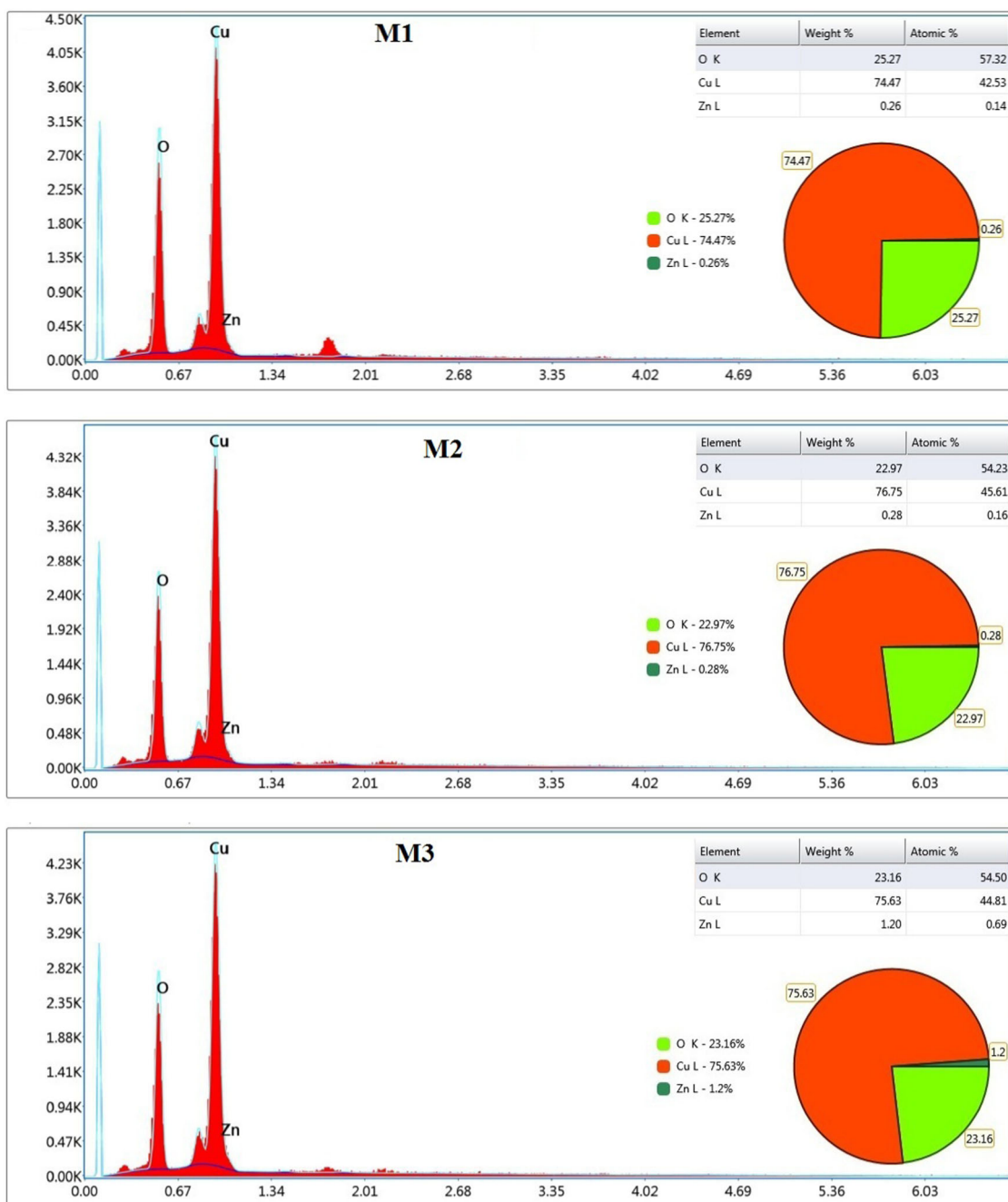


Fig. 9 EDS spectra and elemental analysis for CuO:Zn thin films produced using the manual NSP systems

shown in Fig. 12. The Tauc plot relation is given by

$$\alpha h\nu = A(h\nu - E_g)^n \tag{4}$$

where the absorbance coefficient (α) is estimated from the optical spectra using the relation $\alpha = 2.303 A/t$ where A is absorbance and t is the thickness of the films [40–45]. The optical bandgap energies (E_g) calculated from the Tauc plots were found to be 2.02, 2.05, and 2.12 eV for samples M1, M2, and M3, respectively, and 2.13, 1.90, and 2.18 eV for samples A1, A2, and A3, respectively. From these data,

it is observed that the lowest value of E_g was recorded for sample A2. These studies indicate that at the highest dopant levels, the thin films prepared by the automated NSP system show increased optical absorbance and reduced optical bandgap values when compared with those produced using the manual system.

3.4 DC electrical studies

Figure 13 shows the I–V characteristics of the CuO:Zn thin films. All films exhibited a good current response with

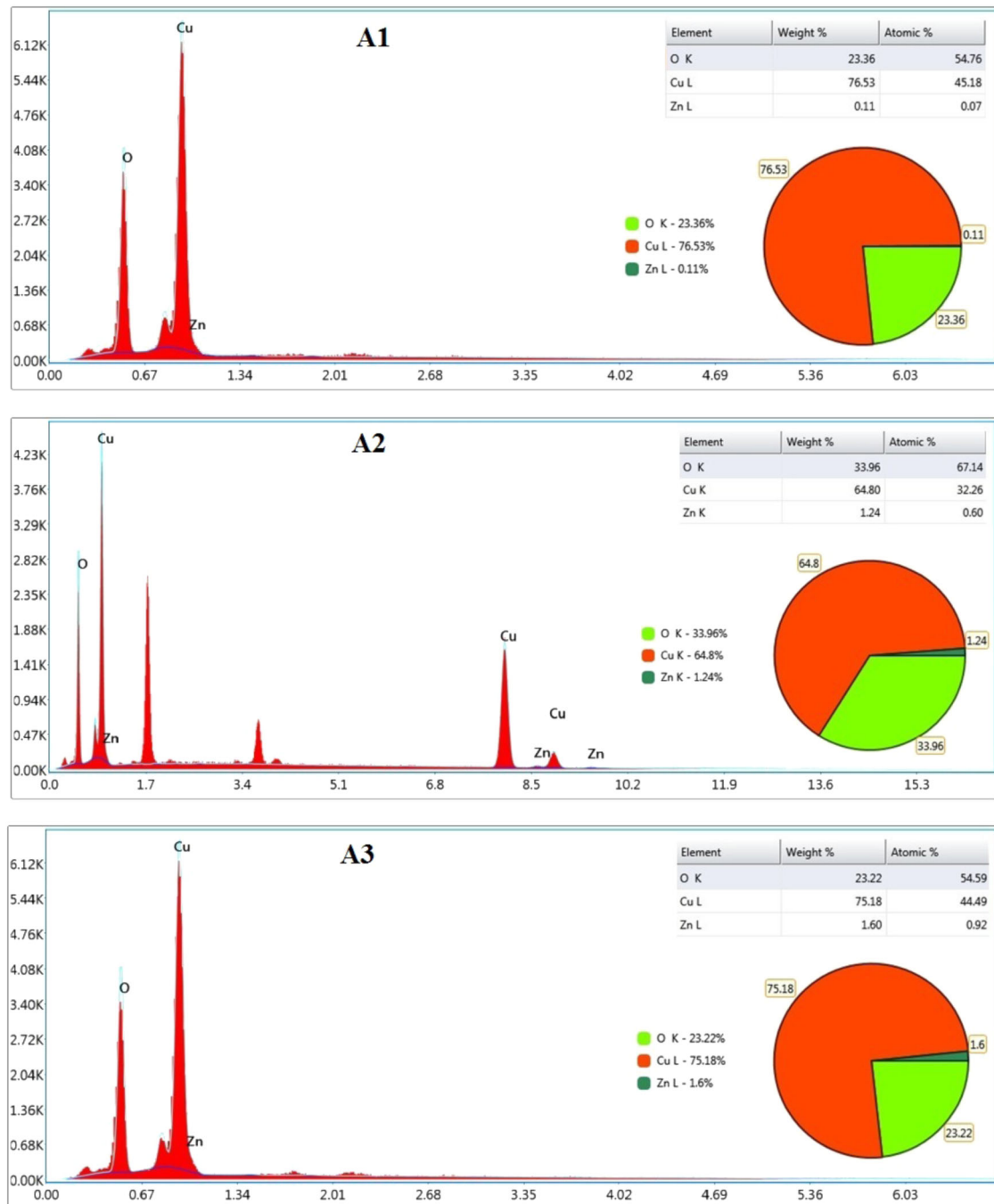


Fig. 10 EDS spectra and elemental analysis for CuO:Zn thin films produced using the automated NSP systems

applied voltage, with samples M2 and A2 exhibiting the highest currents at each voltage. In addition, the samples prepared using the automated NSP system exhibited higher current values than the corresponding samples prepared using the manual NSP system. The average conductivities of the samples are illustrated in Fig. 14. It is evident that the conductivities in the M- and A-sample series exhibit maximum values for samples M2 and A2 of 6.67×10^{-10} and 3.67×10^{-8} S/cm, respectively, with the value for the latter being over 50 times higher than the former.

3.5 I–V characterization of Ag/p-CuO:Zn/n-Si heterojunction diode

The performance and photodetector properties of the heterojunction diode fabricated from the CuO:Zn films can be analyzed by current–voltage (I–V) measurement under light and dark conditions to obtain the ideality factor (η) and barrier height (ϕ_b) of the diode. In our work, a Ag/p-CuO:Zn/n-Si heterojunction diode was fabricated based on the above characterization studies, which indicated that samples

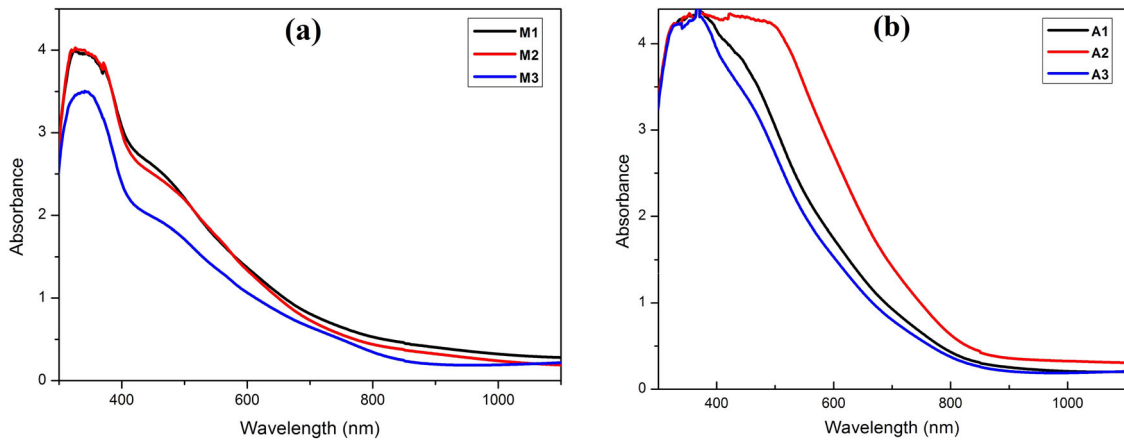


Fig. 11 Optical absorption of CuO:Zn thin films produced using (a) manual and (b) automated NSP systems

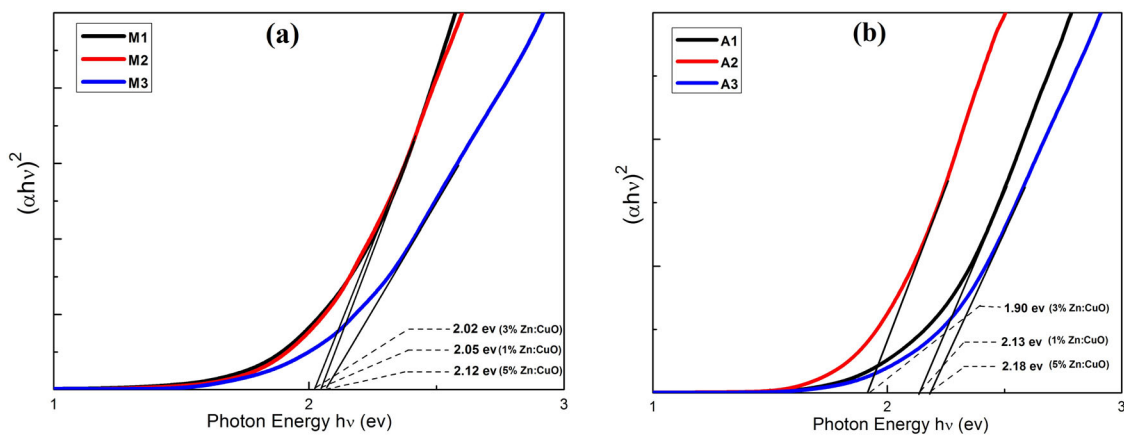


Fig. 12 Optical bandgap of CuO:Zn thin films produced using (a) manual and (b) automated NSP systems

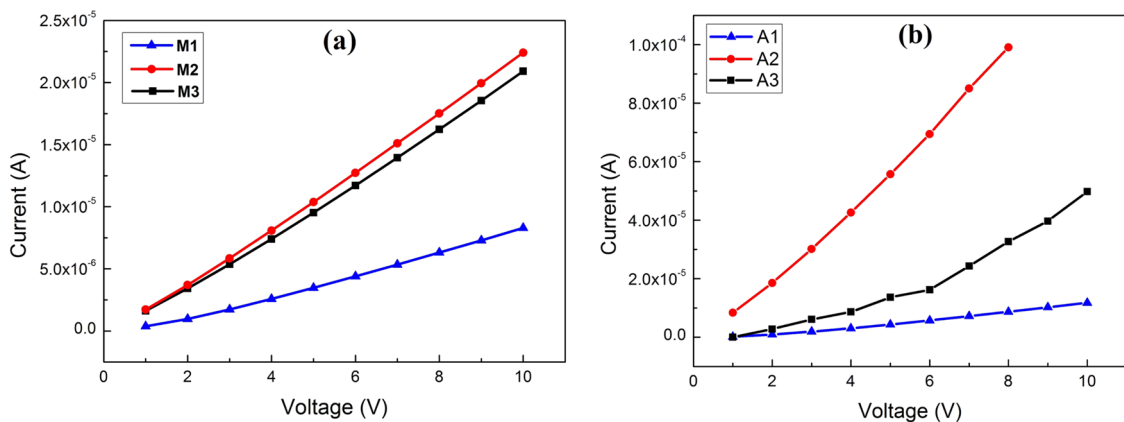


Fig. 13 I–V characterization of CuO:Zn thin films produced using (a) manual and (b) automated NSP systems

M2 and A2 (3% CuO:Zn) exhibited the most suitable properties for incorporating into heterojunction diodes. Figure 15(a, b) illustrate the forward- and reverse-bias I–V characteristics of the heterojunction diodes fabricated using the manual and automated NSP systems. Both devices

measured under light condition exhibit higher current values than under dark conditions. This performance shows that both devices are highly photoconducting in nature. In particular, the diode fabricated using the automated NSP systems shows higher current values when compared to the

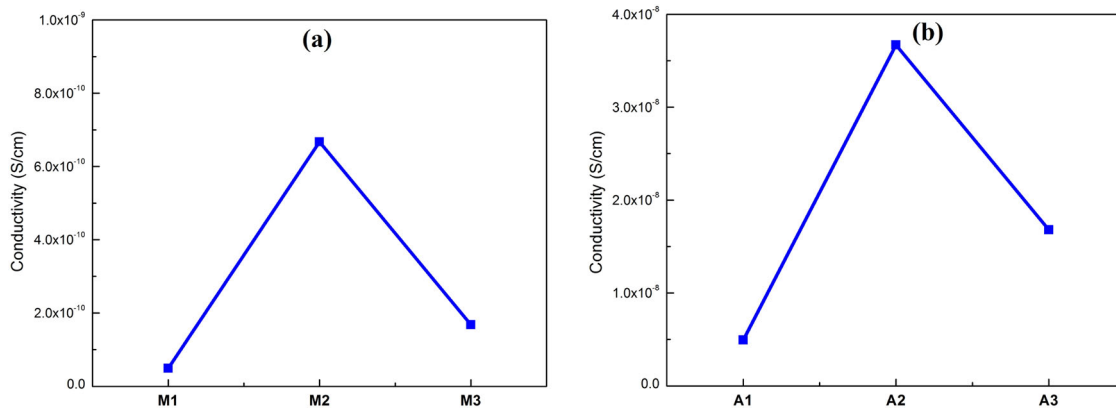


Fig. 14 Average conductivity of CuO:Zn thin films produced using (a) manual and (b) automated NSP systems

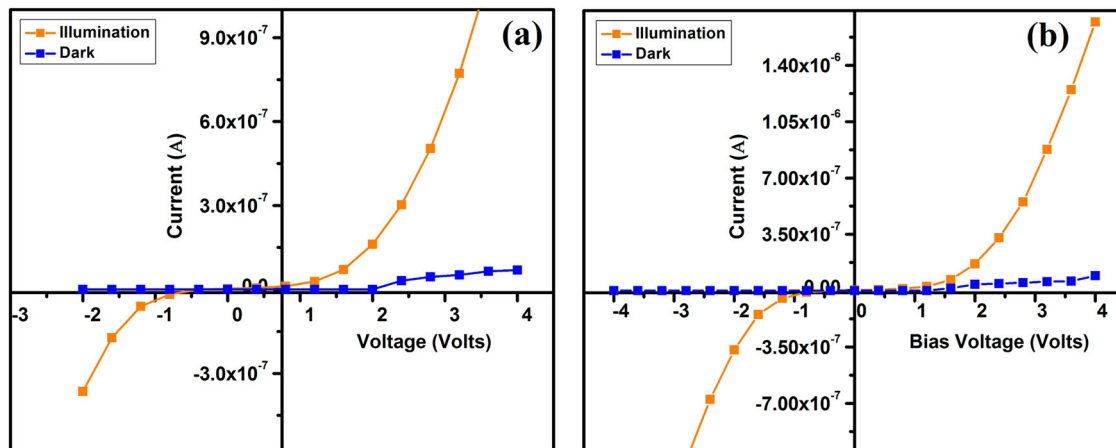


Fig. 15 I–V characteristics of Ag/p-CuO:Zn/n-Si heterojunction diodes produced using (a) manual and (b) automated NSP systems

other diode. As observed in Fig. 13, both devices exhibit maximum current values of 3.28×10^{-9} A (Fig. 15(a)) and 1.38×10^{-8} A (Fig. 15(b)) at relatively low forward-bias voltage (V) under light conditions.

The current density of the heterojunction diodes can be calculated using the thermionic emission (TE) equation [46]:

$$I = I_0 \exp\left(\frac{qV}{nK_bT} - 1\right) \tag{5}$$

where I_0 , q , η , K_b , V , and T are reverse saturation current density, electron charge, ideality factor, Boltzmann constant, applied voltage, and absolute temperature.

The ideality factors (η) of the devices was calculated from the intercepts of semilog plots of the current density ($\ln J$) Vs voltage (V) as shown in Fig. 16. Table 2 summarizes the key diode parameters, namely the ideality factor (η) and barrier height (ϕ_b) under dark and light conditions. It is evident that the ideality factor of the diode decreases with illumination, which indicates the photoconducting behavior of the device. The results also reveal that the diode fabricated using the automated NSP system has a lower

ideality factor and barrier height than that produced using the manual NSP system, with the calculated η value for both devices being higher than the ideal value ($n = 1$, for an ideal P–N diode). The relatively high value of η reflects the nonideal behavior of both devices and may arise from the voltage drop across the layers, the presence of a thin interfacial native oxide layer (SiO_2), and/or recombination due to current and barrier inhomogeneities [47–49].

The ideality factor (η) and barrier height (ϕ_b) values are in good agreement with previous reports, which are summarized in Table 3. The calculated η and ϕ_b values for the Ag/p-CuO:Zn/n-Si devices produced via manual NSP were found to be 4.25 and 0.70 eV, respectively, under dark conditions; and 4.08 and 0.69 eV, respectively, under illumination. The corresponding values obtained using the automated system were 3.32 and 0.68 eV, respectively, under dark conditions; and 3.19 and 0.67 eV, respectively, under illumination. For comparison, Tombak et al. reported 3.5 and 0.96 eV under illumination for Ag/p-CuO/n-Si, while Venkateshwari reported the highest η values of 6.2 and 4.6 under dark and light conditions for p-CuO/n-Si

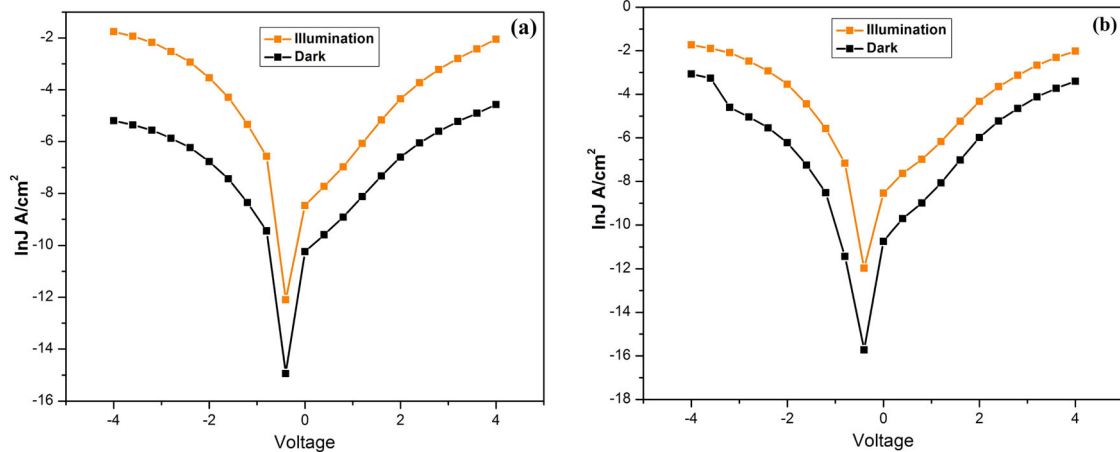


Fig. 16 Semilog plot of the current density ($\ln J$) vs voltage (V) of Ag/p-CuO:Zn/n-Si heterojunction diodes produced using (a) manual and (b) automated NSP systems

Table 2 Selected parameters of Ag/p-CuO:Zn/n-Si heterojunction diode under dark and light condition

Parameters	Manual p-CuO:Zn/n-Si junction diode		Automated p-CuO:Zn/n-Si junction diode	
	Dark	Light	Dark	Light
Ideality factor (η)	4.25	4.08	3.32	3.19
Barrier height (Φ_b) (eV)	0.702	0.691	0.686	0.674

Table 3 Comparison of the Ag/p-CuO:Zn/n-Si heterojunction diode performance with previous reports

Device structure	Ideality factor (η)		Barrier height (Φ_b) (eV)		Reference
	Dark	Light	Dark	Light	
Manual Ag/p-CuO:Zn/n-Si	4.25	4.08	0.702	0.691	Present work
Automated Ag/p-CuO:Zn/n-Si	3.32	3.19	0.686	0.674	Present work
Ag/p-CuO/n-Si	-	3.5	-	0.96	[50]
p-CuO/n-Si	6.2	4.6	0.80	0.81	[51]
Ce-WO ₃ /p-Si	13.33	6.47	0.69	0.702	[52]
n-AlZnO/p-Si	4.32	3.69	-	-	[53]

[50, 51]. Additionally, Marnadu reported η values of 13.33 and 6.47 under dark and light conditions for Ce-WO₃/p-Si, while Kalidass obtained values of 4.32 and 3.69 for n-AlZnO/p-Si [52, 53]. Remarkably, the Ag/p-CuO:Zn/n-Si heterojunction diode produced in this work using the automated system exhibited the lowest η value under light and dark conditions when compared with previous literature reports. Furthermore, the estimated Φ_b values were also

found to be low for the diode produced using the automated system.

4 Conclusion

A microcontroller-based automated NSP system has been designed and developed for depositing thin films. CuO:Zn thin films with doping concentrations of 1%, 3%, and 5% were deposited using the new system, and their properties compared with the corresponding films produced using a conventional manual system. All samples were assigned to the monoclinic crystal phase on the basis of XRD studies. The lowest crystallite sizes were obtained for the samples with 3% dopant (9 and 13 nm for films produced using the automated and manual NSP systems, respectively); these samples also exhibited the highest microstrain and dislocation densities. FESEM studies indicated that more uniform, fine-grained films were obtained using the automated system. The highest optical absorbances and lowest band gaps were observed at dopant levels of 3%, with increasing Zn content, leading to a corresponding increase in the magnitude of the bandgap. The optical studies revealed that films produced using the automated NSP system exhibited higher optical absorbances and lower bandgaps than those obtained via the manual NSP system.

Films deposited using the automated NSP system also exhibited higher conductivity than those prepared using the manual NSP system, with maximum values of 3.67×10^{-8} and 6.67×10^{-10} S/cm, respectively, being obtained at 3% dopant levels. These films were subsequently used to fabricate Ag/p-CuO:Zn/n-Si heterojunction diodes, which were studied under dark and light conditions. The results revealed that the device produced using the automated NSP system

exhibited a lower ideality factor and barrier height than the corresponding device fabricated via the manual NSP.

Overall, the various results confirmed that the automation process in the NSP system significantly improves and modifies the properties of CuO:Zn thin films and Ag/p-CuO:Zn/n-Si heterojunction diode.

Compliance with ethical standards

Conflict of interest The authors declare no competing interests.

Publisher's note Springer Nature remains neutral with regard to jurisdictional claims in published maps and institutional affiliations.

References

- Erkan Y, Mustafa S (2020) Functionalized nanomaterials for sample preparation methods Handbook of nanomaterials in analytical chemistry. Elsevier. <https://doi.org/10.1016/B978-0-12-816699-4.00015-3>
- Jacob A, Andrade-Arvizu MC-P, Osvaldo V-G (2015) SnS-based thin film solar cells: perspectives over the last 25 years. *J Mater Sci Mater Electron* 26:4541–4556. <https://doi.org/10.1007/s10854-015-3050-z>
- Perednis D, Gauckler LJ (2004) Thin film deposition using spray pyrolysis. *J Electroceram* 14:103–111. <https://doi.org/10.1007/s10832-005-0870-x>
- Elfakir A, Tlemçani TS, Benamar EB et al. (2015) Structural, electrical and optical properties of sprayed Nd-F codoped ZnO thin films. *J Sol-Gel Sci Technol* 73:557–562. <https://doi.org/10.1007/s10971-014-3518-y>
- Shashidhar R, Choudhary N (2020) Cost-effective SnS heterojunction solar cells synthesized by spray pyrolysis. *J Sol-Gel Sci Technol* 96:188–196. <https://doi.org/10.1007/s10971-020-05397-7>
- Kathalingam A, Kesavan K, Mary Pradeepa V et al. (2020) Fabrication and characterization of CuO/CdS heterostructure for optoelectronic applications. *J Sol-Gel Sci Technol* 96:178–187. <https://doi.org/10.1007/s10971-020-05391-z>
- Kumar A, Prajapati CS, Sahay PP (2019) Modification in the microstructural and electrochromic properties of spray-pyrolysed WO₃ thin films upon Mo doping. *J Sol-Gel Sci Technol* 90:281–295. <https://doi.org/10.1007/s10971-019-04960-1>
- Mageshwari K, Sathyamoorthy R (2013) Organic free synthesis of flower-like hierarchical CuO microspheres by reflux condensation approach. *Appl Nanosci* 3:161–166. <https://doi.org/10.1007/s13204-012-0116-6>
- Shunmugam M, Gurusamy H, Devarajan PA (2017) Investigations on the structural, electrical properties and conduction mechanism of CuO nano flakes. *Int J Nano Dimens* 8:216–223
- Wang C, Zeng W, Zhang H et al. (2014) Synthesis and growth mechanism of CuO nanostructures and their gas sensing properties. *J Mater Sci: Mater Electron* 25:2041–2046. <https://doi.org/10.1007/s10854-014-1837-y>
- Xiaodi LIU, Guangyin LIU, Lijuan WANG, Yinping LI, Yupei MA, Jianmin MA (2016) Morphology- and facet-controlled synthesis of CuO micro/nanomaterials and analysis of their lithium ion storage properties. *J Power Sources* 312:199–206. <https://doi.org/10.1016/j.jpowsour.2016.02.048>
- Khøjier K, Savaloni H, Sadeghi Z (2014) A comparative investigation on growth, nanostructure and electrical properties of copper oxide thin films as a function of annealing conditions. *J Theor Appl Phys* 8:116. <https://doi.org/10.1007/s40094-014-0116-x>
- K.G. D, Jampana N (2016) Development of an automated ultrasonic spray pyrolysis system and the growth of Cu₂ZnSnS₄ thin films. *J Anal Appl Pyrol* 117:141–146. <https://doi.org/10.1016/j.jaap.2015.12.004>
- Ravichandran K, Manivasha A, Subha K, Chandrabose A, Mariappan R (2016) Cost-effective nebulizer sprayed ZnO thin films for enhanced ammonia gas sensing – Effect of deposition temperature. *Surf Interfaces* 1-3:13–20. <https://doi.org/10.1016/j.surfin.2016.06.004>
- Munjer MA, Hossain MdFaruk, Rahman DrMdHafizur, Mahmud MZ (2012) Fabrication of a cost effective automatic controller for spray-pyrolysis technique to deposit thin films. 7th International Conference on Electrical and Computer Engineering, ICECE 2012. 2012:78–81. <https://doi.org/10.1109/ICECE.2012.6471489>
- Sangle NS, Dhatrak SE, Wagh VG (2015) Microcontroller based solution delivery pump for spray pyrolysis international journal of emerging technology and advanced engineering, Volume 5, Issue 1, 319–322.
- Marabelli F, Parravicini GB, Salghetti-Drioli F (1995) Optical band gap of CuO. *Phys Rev B* 52(3):1433–1436. <https://doi.org/10.1103/PhysRevB.52.1433>
- Ghosh S, Avasthi DK, Shah P, Ganesan V, Gupta A, Sarangi D, Bhattacharya R, Assmann W (2000) Deposition of thin films of different oxides of copper by RF reactive sputtering and their characterization. *Vacuum* 57:377–385. [https://doi.org/10.1016/S0042-207X\(00\)00151-2](https://doi.org/10.1016/S0042-207X(00)00151-2)
- Faiz H, Siraj K, Rafique MS, Naseem S, Anwar AW (2015) Effect of zinc induced compressive stresses on different properties of copper oxide thin films. *Indian J Phys* 89:353–360. <https://doi.org/10.1007/s12648-014-0597-0>
- Baturay S, Tombak A, Kaya D, Ocak YS, Tokus M, Aydemir M, Kilicoglu T (2016) Modification of electrical and optical properties of CuO thin films by Ni doping. *J Sol-Gel Sci Technol* 78:422–429. <https://doi.org/10.1007/s10971-015-3953-4>
- Bayansal F, Taşköprü T, Şahin B, Cetinkara H (2014) Effect of cobalt doping on nanostructured CuO thin films. *Met Mat Trans A* 45:3670–3674. <https://doi.org/10.1007/s11661-014-2306-1>
- Gulen Y, Bayansal F, Sahin B, Cetinkara HA, Guder HS (2013) Fabrication and characterization of Mn-doped CuO thin films by the SILAR method. *Ceram Int* 39:6475–6480. <https://doi.org/10.1016/j.ceramint.2013.01.077>
- Sonia S, Annsi IJ, Kumar PS, Mangalaraj D, Viswanathan C, Ponpandian N (2014) Hydrothermal synthesis of novel Zn doped CuO nanoflowers as an efficient photodegradation material for textile dyes. *Mater Lett* 144:127–130. <https://doi.org/10.1016/j.matlet.2015.01.026>
- Jayaprakash J, Srinivasan N, Chandrasekaran P, Girija EK (2015) Synthesis and characterization of cluster of grapes like pure and Zinc-doped CuO nanoparticles by sol–gel method. *Spectrochim Acta Part A* 136(C):1803–1806. <https://doi.org/10.1016/j.saa.2014.10.087>
- Eshed Michal, Lellouche Jonathan, Gedanken Aharon, Banin Ehud (2014) A Zn-Doped CuO nanocomposite shows enhanced antibiofilm and antibacterial activities against streptococcus mutans compared to nanosized CuO. *Adv Funct Mater* 24(10):1382–1390. <https://doi.org/10.1002/adfm.201302425>
- Yang SG, Li T, Gu BX, Du YW, Sung HY, Hung S T ST, Wong CY, Pakhomov AB (2003) Ferromagnetism in Mn-doped CuO. *Appl Phys Lett* 83:3746. <https://doi.org/10.1063/1.1623944>
- Morales Julian, Sánchez Luis, Martín Francisco, Barrado Jose, Sánchez Miguel (2004) Nanostructured CuO thin film electrodes prepared by spray pyrolysis: a simple method for enhancing the electrochemical performance of CuO in lithium cells. *Electrochim Acta* 49:4589–4597. <https://doi.org/10.1016/j.electacta.2004.05.012>

28. Thangaraju D, Marnadu R, Vedi S, Durairajan A, Ponnusamy K, Chandrasekaran J, Jayakumar S, Valente MA, Greenidge D (2020) Solvent influenced synthesis of single-phase SnS₂ nanosheets for solution-processed photodiode fabrication. *Cryst Eng Comm* 22:525–533. <https://doi.org/10.1039/C9CE01417A>
29. Jagadeesan V, Subramaniam V (2019) Impact of molarity on structural, optical, morphological and electrical properties of copper oxide thin films prepared by cost effective jet nebulizer spray pyrolysis technique. *J Mater Sci: Mater Electron* 30:1571–1578. <https://doi.org/10.1007/s10854-018-0428-8>
30. Sonia S, Annsi I, Kumar J, Mangalaraj DPS, Viswanathan C (2015) Hydrothermal synthesis of novel Zn doped CuO nanoflowers as an efficient photodegradation material for textile dyes *Mater Lett* 144:127–130. <https://doi.org/10.1016/j.matlet.2015.01.026>
31. Cullity BD: *Elements of X-rays*, 2nd ed. Addison Wesley, London (1978)
32. Fan H, Yang L, Hua W, Wu X, Wu Z, Xie S, Zou B (2004) Controlled synthesis of monodispersed CuO nanocrystals. *Nanotechnology* 15:37–42. <https://doi.org/10.1088/0957-4484/15/1/007>
33. Rafea MA, Roushdy N (2009) Determination of the optical band gap for amorphous and nanocrystalline copper oxide thin films prepared by SILAR technique. *J Phys D* 42:015413–015418. <https://doi.org/10.1088/0022-3727/42/1/015413>
34. Baturay S, Tombak A, Kaya D et al. (2016) Modification of electrical and optical properties of CuO thin films by Ni doping. *J Sol-Gel Sci Technol* 78:422–429. <https://doi.org/10.1007/s10971-015-3953-4>
35. Nesa M, Sharmin M, Hossain KS et al. (2017) Structural, morphological, optical and electrical properties of spray deposited zinc doped copper oxide thin films. *J Mater Sci: Mater Electron* 28:12523–12534. <https://doi.org/10.1007/s10854-017-7075-3>
36. Rejith S, Krishnan C (2013) Optical, thermal and magnetic studies on zinc-doped copper oxide nanoparticles. *Mater Lett* 106:87–89. <https://doi.org/10.1016/j.matlet.2013.04.108>
37. Siraj K, Faiz H, Rafique, S. MS (2015) Naseem microstructural and optical properties of zinc doped copper oxide thin films. *Mater Today: Proc* 2:5426–5429. <https://doi.org/10.1016/j.matpr.2015.11.063>
38. Yathisha RO, Arthoba Nayaka Y (2018) Structural, optical and electrical properties of zinc incorporated copper oxide nanoparticles: doping effect of Zn. *J Mater Sci* 53:678–691. <https://doi.org/10.1007/s10853-017-1496-5>
39. Elangovan E, Ramamurthi K (2005) Studies on micro-structural and electrical properties of spray-deposited fluorine-doped tin oxide thin films from low-cost precursor. *Thin Solid Films* 476:231–236. <https://doi.org/10.1016/j.tsf.2004.09.022>
40. Chand P, Gaur A, Kumar A, Gaur UK (2015) Effect of NaOH molar concentration on morphology, optical and ferroelectric properties of hydrothermally grown CuO nanoplates. *Mater Sci Semicond Process* 38:72–80. <https://doi.org/10.1016/j.mssp.2015.04.006>
41. Anu Prathap MU, Kaur B, Srivastava R (2012) Hydrothermal synthesis of CuO micro-/nanostructures and their applications in the oxidative degradation of methylene blue and non-enzymatic sensing of glucose/H₂O₂. *J Colloid Interface Sci* 370:144–154. <https://doi.org/10.1016/j.jcis.2011.12.074>
42. Jana S, Das S, Das NS, Chattopadhyay KK (2010) CuO nanostructures on copper foil by a simple wet chemical route at room temperature. *Mater Res Bull* 45:693–698. <https://doi.org/10.1016/j.materresbull.2010.02.014>
43. Borgohain K, Mahamuni S (2002) Formation of Single-phase CuO Quantum Particles. *J Mater Res* 17:1220–1223. <https://doi.org/10.1557/JMR.2002.0180>
44. Raja Muthusamy, Chandrasekaran J, Murugan Balaji, Balasundaram Janarthanan (2016) Impact of annealing treatment on structural and dc electrical properties of spin coated tungsten trioxide thin films for Si/WO₃/Ag junction diode. *Mater Sci Semicond Process* 56:145–154. <https://doi.org/10.1016/j.mssp.2016.08.007>
45. Hong Kihyon, Kim Kisoo, Kim Sungjun, Lee Illhwan, Cho Hyunsu, Yoo Seunghyup, Choi HoWon, Lee Nam-Yang, Tak Yoon-Heung, Lee Jong-Lam(2011) Optical properties of WO₃/Ag/WO₃ multilayer as transparent cathode in top-emitting organic light emitting diodes. *J. Phys. Chem. C* 115(8):3453–3459. <https://doi.org/10.1021/jp109943b>
46. Katate T, Onozato T, Hirono M et al. (2016) A transparent electrochromic metal-insulator switching device with three-terminal transistor geometry. *Sci Rep.* 6:25819. <https://doi.org/10.1038/srep25819>
47. Tataroglu A, Altindal S (2006) Characterization of current–voltage (I–V) and capacitance–voltage–frequency (C–V–f) features of Al/SiO₂/p-Si (MIS) Schottky diodes. *Microelectr Eng* 83(3):582–588
48. Card HC, Rhoderick EH (1971) Studies of tunnel MOS diodes I. Interface effects in silicon Schottky diodes. *J Phys D: Appl Phys* 4:1589. <https://doi.org/10.1088/0022-3727/4/10/319>
49. Wang CX, Yang GW, Liu HW, Han YH, Luo JF, Gao CX, Zou GT (2004) Experimental analysis and theoretical model for anomalously high ideality factors in ZnO/diamond p-n junction diode. *Appl Phys Lett* 84:2427. <https://doi.org/10.1063/1.1689397>
50. Tombak A, Benhaliliba M, Ocak Y, & Kılıçoğlu T (2016) The novel transparent sputtered p-type CuO thin films and Ag/p-CuO/n-Si Schottky diode applications. *Results in Physics*. 5. <https://doi.org/10.1016/j.rinp.2015.11.001>.
51. Venkateswari, P, Thirunavukkarasu P, Ramamurthy M, Murugan B, Chandrasekaran J (2017) Optimization and characterization of CuO thin films for P-N junction diode application by JNSP technique. *Optik-International Journal for Light and Electron Optics*. 140. <https://doi.org/10.1016/j.ijleo.2017.04.039>.
52. Marnadu R, Chandrasekaran J, Maruthamuthu S, Balasubramani V, Vivek P (2019) Ultra-high photoresponse with superiorly sensitive metal-insulator-semiconductor (MIS) structured diodes for UV photodetector application. *Appl Surf Sci* 480:308–322. <https://doi.org/10.1016/j.apsusc.2019.02.214>
53. Kalidass S, Thirunavukkarasu P, Balaji M, Chandrasekaran J (2018) Investigation on Al doped ZnO thin films and its N-Al₂O₃/P-Si junction diodes via dip coating and JNSP techniques. *Orient J Chem* 34.